THE JOURNAL OF PHYSICAL CHEMISTRY C

Article

pubs.acs.org/JPCC

Efficient Co-Nanocrystal-Based Catalyst for Hydrogen Generation from Borohydride

Bingrui Liu,[†] Alyssa Rose,[‡] Ning Zhang,[†] Yan-Yan Hu,*[,‡] and Mingming Ma*[,†]

[†]CAS Key Laboratory of Soft Matter Chemistry, iChEM (Collaborative Innovation Center of Chemistry for Energy Materials), Department of Chemistry, University of Science and Technology of China, Hefei, Anhui 230026, People's Republic of China

[‡]Department of Chemistry and Biochemistry, Florida State University, Tallahassee, Florida 32306, United States

Supporting Information

ABSTRACT: Sodium borohydride ($NaBH_4$) has been proposed as a potential hydrogen storage material for fuel cells, and the development of highly active and robust catalysts for hydrolyzing $NaBH_4$ is the key for the practical usage of $NaBH_4$ for fuel cells. Herein we report Co-nanocrystal assembled hollow nanoparticles (Co-HNP) as an active and robust catalyst for the hydrolysis of $NaBH_4$. A hydrogen generation rate of 10.8 $L \cdot min^{-1} \cdot g^{-1}$ at 25 °C was achieved by using the Co-HNP catalyst with a low activation energy of 23.7 $kJ \cdot mol^{-1}$, which is among the best performance of reported noble and non-noble catalysts for hydrolyzing $NaBH_4$. Co-HNP also showed good stability in the long term cycling tests. The mechanism of the catalytic hydrolysis of $NaBH_4$ on Co-HNP was studied by using ^1H and ^{11}B solid-state NMR, which provided unambiguous experimental evidence of the Co−H formation. The systematically designed NMR experiments unveiled the key role of Co-HNP in the activation of borohydride and the subsequent transfer of H^- to water for generating H_2 gas and helped to distinguish various hypotheses proposed for catalytic H_2 generation reactions. The porous hollow nanostructure of the Co-HNP catalyst provides large surface area and facilitates mass transfer. The facile preparation and outstanding performance of Co-HNP enables it as a very competitive catalyst for hydrogen production.

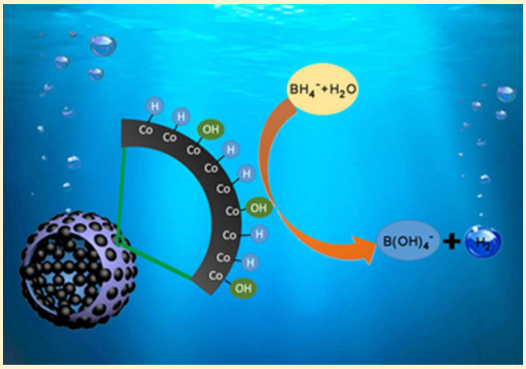

INTRODUCTION

Hydrogen is considered a promising alternative energy source to fossil fuels due to its cleanness, high energy density, and high energy conversion efficiency when used in fuel cells.[1] However, the use of hydrogen as a fuel is hindered by the lack of safe and efficient technology for hydrogen storage and transportation.[2] Sodium borohydride ($NaBH_4$, SBH) possesses a hydrogen capacity of 10.8 wt % and can be safely stored in basic aqueous solutions. The hydrogen generation can be initiated on demand by adding a catalyst to SBH-containing solutions with a controlled hydrolysis rate.[3] Thus, SBH has been proposed as a potential hydrogen storage material, especially for supplying hydrogen to fuel cells.[4]

Various catalysts have been explored to control the hydrolysis reaction of SBH, including noble metals (e.g., Ru,[5] Pt[6] and Pd[7]), iron group metals[8] (e.g., Co, Ni and Fe) and metal alloys (e.g., Co−P,[9] Co−B,[10] Co−P−B,[11] and Co−Ni−P−B[12]). While noble metal catalysts show excellent catalytic activity, their applications have been restricted by their high cost and limited supply. Alternatively, non-noble metal (especially Co and Ni)-based catalysts for hydrolysis of SBH have been developed, and their activity can be further improved by dopants such as P, B, non-noble metals,[13] or noble metals.[14] Besides doping, the activity of Co- and Ni-based catalysts can also be improved by creating porous structures (e.g., Raney Ni,[15] Co−B,[16,17] and Co−Ni−P[18]). However, the catalytic activity of current Co- and Ni-based catalysts for SBH hydrolysis is still lower than that of noble metal-based catalysts (see Table S1 for comparison). The development of highly active and robust non-noble metal-based catalysts for SBH hydrolysis is desired, but remains a challenge.[3]

In this paper, we adapt our previously developed method to synthesize cobalt-nanocrystal-assembled hollow nanoparticles (Co-HNP),[19] and demonstrate the outstanding performance of Co-HNP as catalysts for the hydrolysis of SBH. At room temperature, a hydrogen generation rate of 10.8 $L \cdot min^{-1} \cdot g^{-1}$ from Co-HNP-catalyzed SBH hydrolysis was achieved. The apparent activation energy for the hydrolysis of SBH was determined to be 23.7 $kJ \cdot mol^{-1}$. The performance of Co-HNP is among the best of reported noble and non-noble catalysts for this reaction (see Table S1 for comparison). Co-HNP also showed good stability in the cycling test. The high performance of Co-HNP catalyst is attributed to the synergistic effect between Co and doping elements, together with the porous hollow nanostructure of Co-HNP, which provides large surface area and facilitates mass transfer.

Received: March 31, 2017
Revised: May 22, 2017
Published: May 23, 2017

DOI: 10.1021/acs.jpcc.7b03094
J. Phys. Chem. C 2017, 121, 12610−12616

In addition, various mechanisms have been proposed to explain the catalytic reactions for generating H_2,[13,20] and most of them are based on investigating the kinetics and thermodynamics. More direct experimental evidence is necessary to identify the intermediate species formed during the reaction, which will lead to a more convincing proposal of the reaction mechanism and will help to support or dispute previously proposed reaction mechanisms. In order to obtain direct experimental data to delineate the mechanism of Co-HNP catalyzed SBH hydrolysis, solid-state ^1H and ^{11}B NMR was employed to probe the changes of ^1H and ^{11}B local environments. The methodically designed and performed NMR experiments have unambiguously revealed the critical role of Co-HNP in the activation of SBH by forming Co−H and in the transfer of H^- to H_2O to form H_2 gas.

EXPERIMENTAL SECTION

Reagents and Materials. All the chemical reagents were purchased from Sinopharm Chemical Reagent Co. Ltd., and used as received. All the solutions were prepared with ultrapure water. A probe sonicator from Scientz Inc. (model IID) was used for the synthesis of Co-HNP and Co-SNP with a fixed output power of 10 W when applied to a 20 mL reaction solution.

Synthesis of Cobalt Nanocrystal Assembled Hollow Nanoparticles (Co-HNP). The synthesis of Co-HNP was performed according to literature.[19] Briefly, 0.119 g of $CoCl_2 \cdot 6H_2O$, 0.099 g of $Na_2WO_4 \cdot 2H_2O$ and 0.136 g of $NaH_2PO_2 \cdot H_2O$ was dissolved in water separately and quickly mixed together under ultrasonic radiation to get a pink turbid solution containing amorphous $CoWO_4$ NPs (20 mL). 0.073 g of solid $NaBH_4$ as a reducing agent was added into the above $CoWO_4$ suspension under ultrasonic radiation. It took 30 min to finish the addition. The reaction solution was cooled in an ice water bath and kept under ultrasonic radiation until no more bubble formation. The black product was collected by centrifugation (8000 rpm for 5 min), and washed with ultrapure water for three times. The obtained Co-HNP product was stored in water until examination.

Synthesis of Cobalt Nanocrystal Assembled Solid Nanoparticles (Co-SNP). The synthesis of Co-SNP was performed according to literature.[19] 0.119 g of $CoCl_2 \cdot 6H_2O$ and 0.136 g of $NaH_2PO_2 \cdot H_2O$ were dissolved in water to give the solution A (15 mL). 0.073 g of $NaBH_4$ and 0.099 g of $Na_2WO_4 \cdot 2H_2O$ were dissolved in water to give the solution B (5 mL). Solution B was slowly added into the solution A under ultrasonic radiation in an ice water bath. It took 20 min to finish the addition. The reaction solution was cooled in an ice water bath and kept under ultrasonic radiation until no more bubble formation. The black product was also collected by centrifugation (8000 rpm for 5 min), and washed with ultrapure water for three times. The Co-SNP product was stored under water until examination.

Synthesis of Amorphous Cobalt-Based Materials (Amorphous-Co) for Comparison. To investigate the effect of ultrasonication on the formation of Co-HNP and Co-SNP, we also prepared a Co-based catalyst without using ultrasonication, from the same reagents as those for synthesizing Co-HNP. Briefly, 0.119 g of $CoCl_2 \cdot 6H_2O$, 0.099 g of $Na_2WO_4 \cdot 2H_2O$, and 0.136 g of $NaH_2PO_2 \cdot H_2O$ were dissolved in water separately and quickly mixed together under stirring to get a 20 mL pink turbid solution. 0.073 g of solid $NaBH_4$ as a reducing agent was added into the above solution under stirring. It took 20 min to finish the addition. The reaction solution was cooled in an ice water bath and finished until no more bubble formation. The black product was collected by centrifugation (8000 rpm for 5 min), and washed with ultrapure water three times. The obtained Amorphous-Co product was stored in water until examination.

Materials Characterization. Field emission scanning electron microscope (FE-SEM, JEOL JSM-6700F) was used to carry out the SEM images. TEM/HRTEM images, SAED patterns were taken with a JEOL JEM-2010 transmission electron microscope with an acceleration voltage of 200 kV. An energy-disperse X-ray spectrum (EDS) was taken on a JEOL JEM-2100F field-emission high-resolution transmission electron microscope operated at 200 kV. X-ray powder diffraction (XRD) was carried out on a Rigaku D X-ray diffractometer with Cu Kα radiation (λ = 1.54178 Å). The X-ray photoelectron spectra (XPS) were recorded on a Thermos ESCALAB 250 using Al Kα (hγ = 1486.6 eV) radiation exciting source. Raman spectrum was recorded on a LABRAM-HR Confocal Laser Micro Raman Spectrometer 750 K with a laser power of 0.5 mW. The nitrogen sorption isotherms were measured by using automatic volumetric adsorption equipment (Micromeritics ASAP 2020). The samples were dried overnight at 100 °C under vacuum before the nitrogen sorption experiment.

Solid State NMR. The ^1H and ^{11}B solid-state magic-angle-spinning (MAS) NMR spectra were acquired on an AVANCE I Bruker spectrometer in a 7 T magnetic field. Samples were packed into 4 mm Bruker MAS rotors and spun at a MAS rate of 10 kHz. A spin−echo NMR pulse sequence was applied with a 90° pulse length of 5.35 ms for ^1H and 4.6 μs for ^{11}B. The recycle delays were 3 s for ^1H and 1 s for ^{11}B. Boron trifluoride diethyl etherate, ($BF_3 \cdot Et_2O$), with a ^{11}B resonance at 0 ppm and ^1H resonance at 1.4 ppm, was used as the chemical shift reference for both ^1H and ^{11}B. The sample preparation for NMR experiments involved centrifuging the Co-HNP/NaOH aqueous solution in 1.5 mL Eppendorf tubes and decanting the excess water to retain a Co-HNP slurry. For the samples treated with Deuterium oxide (D_2O), D_2O was added after the first centrifuge and decantation process. The tube was then agitated and recentrifuged, in order to remove excess D_2O. $NaBH_4$ was added directly to the rotors after packing the Co-HNP slurry. The catalytic reaction between $NaBH_4$ and D_2O/H_2O was highly exothermic and produced a large amount of hydrogen gas, causing bubble formation within the slurry.

Determination of Catalytic Activity and Stability of Catalysts for the Hydrolyzing SBH. The collection of hydrogen was performed by using the water displacement method. 10 mL of aqueous alkaline-stabilized SBH solution (1 wt % SBH, 1 wt % NaOH) was loaded into a round-bottom flask (25 mL) in a water bath, which was connected with an outlet tube. 10 mg of catalyst powder (Co-HNP, Co-SNP or Amorphous-Co) was placed quickly into the flask. The volume of generated hydrogen was recorded when H_2 was collected in an inverted water-filled graduated cylinder. For the recycling test, the used Co-HNP catalyst was retained in the flask by a magnet, while the liquid solution was decanted. Then, another 10 mL aqueous alkaline-stabilized SBH solution was added to the flask without being mixed with the Co-HNP catalyst on the flask wall. When the H_2 collection apparatus was setup, the flask was gently shaken to mix Co-HNP catalyst and the solutions to initiate the H_2 generation reaction.

DOI: 10.1021/acs.jpcc.7b03094
J. Phys. Chem. C 2017, 121, 12610−12616

RESULTS AND DISCUSSION

Synthesis of Co-HNP. Co-HNP was prepared using a "sacrificial template" method (Figure 1a).[19] Amorphous

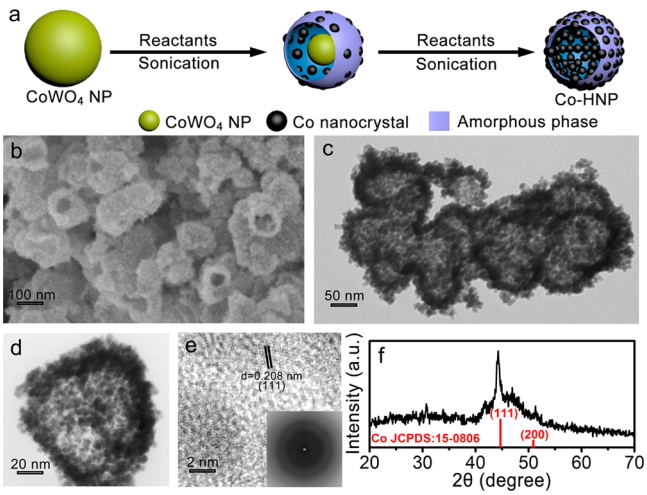

Figure 1. Synthesis and characterization of Co-HNP. (a) Schematic representation of the synthesis of Co-HNP. (b) SEM image, and (c,d) TEM images showing that the shell of the Co-HNP consists of Co nanocrystals and amorphous materials. (e) HRTEM image showing ~5 nm cobalt nanocrystals in fcc phase surrounded by amorphous materials. The inset is the SAED pattern. (f) XRD pattern of Co-HNP; two red lines indicate the standard peaks of Co fcc phase (JCPDS: 15-0806).

$CoWO_4$ NPs were prepared by a precipitation reaction between Co^{2+} and WO_4^{2-} (Figure S1, ~80 nm in diameter). When reduced by borohydride, CoB alloy deposited on the surface of $CoWO_4$ NPs and converted to Co nanocrystals (Co-NC), while the $CoWO_4$ NPs gradually dissolved to form hollow nanoparticles. The extreme but transient local conditions caused by acoustic cavitation could facilitate the conversion from CoB alloy to Co-NC, and the fast dissolution of amorphous $CoWO_4$ NPs.[19]

Characterization of Co-Based Catalysts. The scanning electron microscopy (SEM) image of Co-HNP shows nanoparticles with a diameter around 100 nm (Figure 1b), with some broken ones showing the hollow structure. TEM images show that the diameter of the inside cavity was around 80 nm (Figure 1c,d), consistent with the size of $CoWO_4$ NPs that served as sacrificial templates (Figure S1). High-resolution TEM (HRTEM, Figure 1e) and selected area electron diffraction (SAED, Figure 1e inset) data indicate the crystalline nature of Co-NC with interplane spacing of 0.208 nm, corresponding to the (111) plane of cobalt face-centered cubic (fcc) phase. The two diffraction rings in SAED pattern are associated with the (111) and (110) planes of Co fcc phase (Figure 1e). The powder X-ray diffraction (XRD) of Co-HNP (Figure 1f) shows a broad diffraction peak in the 2θ range between 40° and 50°, with a sharp peak at 2θ = 44° corresponding to cobalt fcc phase (JCPDS No. 15-0806). By using Scherrer equation, the mean diameter of Co-NC was estimated to be 5.5 nm, consistent with the observation by HRTEM (Figure 1e).

The chemical composition of Co-HNP was studied by using XPS (Figure S2) and energy dispersive X-ray spectroscopy (EDX) (Figure S3), which gave the atomic ratio Co:P:W:B = 9.7:1.3:1:6.6. XPS survey also provided valuable information on the chemical status of elements in Co-HNP. In the Co 2p spectrum, two sets of peaks at 776.9/791.7 eV and 780.2/796.1 eV were assigned to Co (0) and Co (II) species, corresponding to Co NC and cobalt oxide,[19] respectively. In the W 4f spectrum, two peaks at 35.8 and 38.0 eV were assigned to W (VI), likely as tungstate, while the peaks at 31.4 and 34.2 eV indicated the existence of metallic W (0) species.[19] In the P 2p spectrum, the peak at 129.3 eV indicated P(0) or phosphide, while the stronger peak at 133.8 eV was attributed to phosphate.[11] The B 1s peak at 187.8 eV was assigned to B (0), while the bigger one locating at 192.1 eV was assigned to borate species.[21] Thus, the XPS data suggests the existence of cobalt oxide, boron oxide or borate, phosphate and tungstate on the surface of Co-HNP, consisting the amorphous oxide layer to protect the Co-NC. This composition of amorphous oxide layer was also confirmed by the Raman spectrum of the Co-HNP sample (Figure S4), where the characteristic vibration peaks of borate, CoO, phosphate and tungstate were observed.

In addition, the XPS peaks of elemental Co (776.9/791.7 eV) and P (129.3 eV) of Co-HNP showed partial negative shifts from the standard values of elemental Co (778.2/793.4 eV) and P (130.2 eV), while the XPS peaks of B (187.8 eV) indicated partial positive shifts from the standard values of elemental B (187.2 eV) (reference data from NIST Database; see Figure S5 for details). These XPS peak shifts suggest electron donation and reception among B, Co, and P atoms, making Co and P electron-rich, and B electron-deficient, which likely comprise the catalytic active sites for hydrolysis of SBH. No peak shift was observed for W (0) and W (VI) peaks, which implies a different role of W. Since W metal and alloys are highly resistant to oxidation, W in the Co-HNP may help to avoid the agglomeration of Co-NC and protect Co-NC from oxidation.

For comparison, Co-NC assembled solid nanoparticles (Co-SNPs) were also synthesized by a simple codeposition method (see Experimental Section for details). The characterization of Co-SNP was performed by using XRD, SEM, TEM (Figure S6), and XPS (Figure S7). The chemical composition of Co-SNP was close to that of the Co-HNP. The size and phase of Co-NCs in Co-SNPs was also similar to that in Co-HNPs. The only one major difference between Co-SNPs and Co-HNPs was the solid versus hollow nanostructure. As shown in Figure S8, the Brunauer–Emmett–Teller (BET) surface area of Co-HNP was 38 $m^2 \cdot g^{-1}$, while the BET surface area of Co-SNP was only 20 $m^2 \cdot g^{-1}$. The pore size in the Co-HNP sample was mainly in the range of 2–10 nm, which was similar to that in Co-SNP sample. The comparison of BET surface area indicates the benefit of hollow nanostructures on providing large surface area for catalytic reactions, as discussed later.

To demonstrate the effect of ultrasonication on the preparation reaction of Co-based catalysts, we also prepared a Co-based catalyst without using ultrasonication, from the same reagents as those for synthesizing Co-HNP. Due to the absence of acoustic cavitation conditions, the reaction between $CoWO_4$ and $NaBH_4$ in the solution was slow. As shown in Figure S9, only some amorphous structure was observed for the obtained Amorphous-Co catalyst. The comparison indicates that ultrasonication not only contributes to the formation of cobalt nanocrystals, but also helps the formation of hollow structure of Co-HNP.

Catalytic Hydrolysis of Sodium Borohydride. The catalytic activities of three Co-based catalysts for SBH hydrolysis were studied by measuring the hydrogen generation

DOI: 10.1021/acs.jpcc.7b03094
J. Phys. Chem. C 2017, 121, 12610–12616

(HG) rate of SBH hydrolysis at 298 K. Figure 2a shows the hydrogen yields of hydrolysis of 1 wt % SBH solution with 1

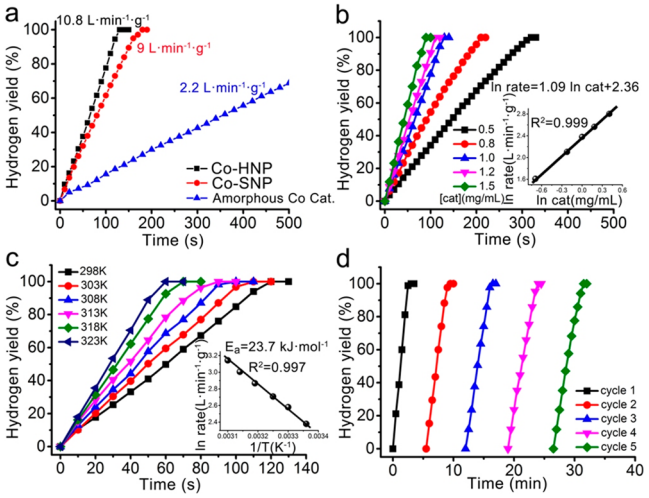

Figure 2. Catalytic performance of Co-HNP for SBH hydrolysis. (a) Hydrogen yield of the SBH hydrolysis (1 wt % solution) with three different Co-based catalysts; (b) the hydrolysis of SBH solution (1 wt %) catalyzed by Co-HNP at different catalyst concentrations; inset: ln[catalyst] vs ln(rate); (c) the hydrolysis of SBH solution (1 wt %) catalyzed by Co-HNP at different temperatures from 298 to 323 K; inset: the Arrhenius plot of the reaction rate; (d) cycling test of Co-HNP catalyst for the hydrolysis of SBH solution (1 wt %).

mg/mL Co-based catalysts (Co-HNP, Co-SNP, or Amorphous-Co). After the addition of catalysts, the hydrolysis of alkaline-stabilized SBH commenced immediately, without any induction period. The average HG rate by Co-HNP was 10.8 $L{\cdot}min^{-1}{\cdot}g^{-1}$, which was larger than that of Co-SNP (9 $L{\cdot}min^{-1}{\cdot}g^{-1}$) or amorphous-Co (2.2 $L{\cdot}min^{-1}{\cdot}g^{-1}$). The catalytic activity of Co-HNP for hydrolysis of SBH is also better than that of most reported non-noble catalysts (Table S1). To probe the effect of NaOH on the sodium borohydrate hydrolysis,[22] we tested the hydrolysis of 1 wt % SBH solution with 1 mg/mL Co-HNP or Co-SNP as the catalyst at different NaOH concentrations. As shown in Figure S10, the HG rates for Co-HNP and Co-SNP reached a maximum (10.8 and 9 $L{\cdot}min^{-1}{\cdot}g^{-1}$, respectively) when the NaOH concentration was 0.25 $mol{\cdot}L^{-1}$, and gradually decreased with the increasing of the NaOH concentration. When the NaOH concentration increased to 2.5 $mol{\cdot}L^{-1}$, the HG rates for Co-HNP and Co-SNP decreased by ~50% (5.5 and 4.6 $L{\cdot}min^{-1}{\cdot}g^{-1}$, respectively). Figure 2b shows the hydrolysis of 1 wt % alkaline-stabilized SBH solution with varied amounts of Co-HNP. The expected increase in the reaction rate with increasing catalyst amount was observed. As shown in the inset of Figure 2b, the logarithmic plot of the calculated reaction rate versus Co-HNP concentration has a slope of 1.09, indicating that the SBH hydrolysis reaction follows first-order kinetics with respect to Co-HNP.[23] In addition, the SBH concentration was also varied and tested (Figure S11). The logarithmic plot of the calculated reaction rate versus SBH concentration showed a slope of 0.057, indicating a zero-order kinetics with respect to SBH (inset of Figure S11).[24] The kinetics result suggests that the SBH hydrolysis is controlled by the catalytic reaction at the active sites of Co-HNP, while the low-concentration active sites are saturated by the relatively high concentration SBH.[25]

As shown in Figure 2c, the Co-HNP catalyzed SBH hydrolysis reaction presented a clear temperature dependence, which was utilized to calculate the apparent activation energy. An Arrhenius plot of ln k (the initial reaction rate) versus the reciprocal of absolute temperature ($1/T$) shows that the activation energy for the SBH hydrolysis on Co-HNP was 23.7 $kJ{\cdot}mol^{-1}$ (inset in Figure 2c). This activation energy is much smaller than that of reported non-noble metal based catalysts (Table S1), demonstrating a very high catalytic activity of Co-HNP for SBH hydrolysis. The reusability of Co-HNP for SBH hydrolysis was tested (see Experimental Section for details). As shown in Figure 2d, Co-HNP retains its high catalytic activity in the cycling test. The XPS spectra and TEM images of Co-HNP catalysts before and after catalyzing SBH hydrolysis were compared in Figure S12, which showed no significant change in both chemical composition and nanostructure of Co-HNP after catalyzing the SBH hydrolysis. The characterization data of postcatalysis Co-HNP clearly indicates its good stability, which agrees with the retention of its high catalytic activity during the cycling test.

Mechanism of Co-HNP Catalyzed SBH Hydrolysis. Currently, the catalytic mechanism by which metal catalysts promote the hydrolysis of SBH is still unclear, due to the difficulties in obtaining direct and convincing evidence to decipher the interaction between solid catalyst and liquid reactants.[13] Therefore, we used methodically designed ^{1}H and ^{11}B solid-state NMR experiments to gain insight into the catalytic hydrolysis process of SBH. Borohydride and water are the two reactants, which should interact with Co-HNP to achieve the critical step of H^- transfer from SBH to H_2O via HNP. There have been indirect evidence suggesting the existence of adsorbed H atoms on metal catalysts.[13]

Here, the hydrogen local environments on the surface of Co-HNP catalyst were examined with ^{1}H NMR. As shown in Figure 3a, the ^{1}H spectrum of Co-HNP exhibits two groups of resonances, one is centered around −2 ppm and the other about 4 ppm. The −2 ppm resonance is assigned to Co−H, as typically only metal hydrides have ^{1}H peaks with negative shifts. The 4 ppm resonance is from $B(OH)_4^-$ hydrogen-bonded to Co−H on the catalyst surface. Once H_2O was added to the Co-HNP catalyst, the Co−H resonance disappeared, and meanwhile two new peaks emerged at 4.8 and 5.5 ppm. The 4.8 ppm resonance is from excess H_2O. The growth of the 5.5 ppm peak at the cost of the Co−H resonance at −2 ppm suggests the reaction of H_2O with Co−H via the following process:

$$Co{-}H + H_2O \rightarrow Co{-}OH + H_2$$

The 5.5 ppm ^{1}H resonance is from OH^-, which sees more significant increase in intensity in the Co-HNP-catalyzed reaction of H_2O and $NaBH_4$.

The solid-state ^{1}H NMR spectrum of $NaBH_4$ shows a major broad resonance centering around −0.2 ppm and another broad peak spanning between 3 and 5 ppm. The large peak width and poor resolution of both resonances are results of strong $^{1}H-^{1}H$ homonuclear dipolar couplings on the order of kHz within $NaBH_4$. The addition of H_2O/D_2O to $NaBH_4$ allows isotopic tumbling of the BH_4^- ions, which averages out $^{1}H-^{1}H$ homonuclear dipolar coupling and yields narrower resonances with significantly improved resolution. The resulting higher-resolution permits the observation of multiplets due to relatively weak J-coupling interactions on the order of Hz. In the ^{1}H NMR of the $NaBH_4 + H_2O/D_2O$ sample, the $NaBH_4$ resonance first splits into four peaks with a J-coupling

DOI: 10.1021/acs.jpcc.7b03094
J. Phys. Chem. C 2017, 121, 12610−12616

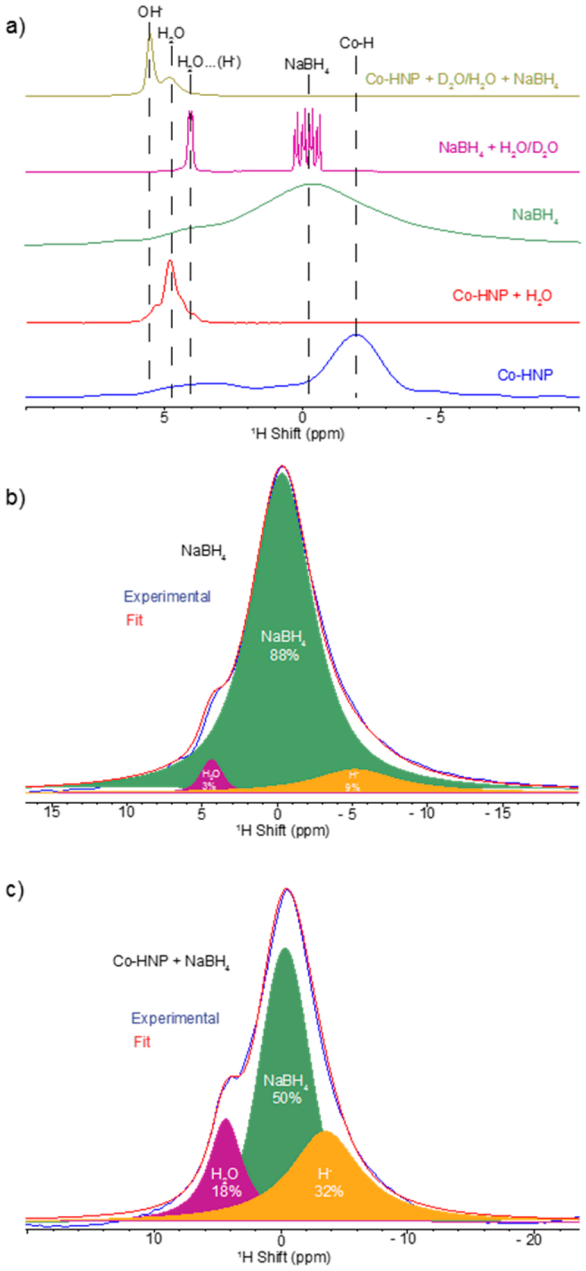

Figure 3. Using solid-state ^{1}H NMR spectra to probe the reaction mechanism of Co-HNP catalyzed SBH hydrolysis. (a) Comparison of solid-state ^{1}H NMR spectra of samples with different combinations of Co-HNP, $NaBH_4$, and H_2O; (b) solid-state ^{1}H spectrum of $NaBH_4$ alone; and (c) solid-state ^{1}H spectrum of Co-HNP + $NaBH_4$.

spacing of 84 Hz from through-bond interactions of ^{1}H and ^{11}B. Then each of the four peaks further splits into 2 with a spacing of 34 Hz, which is due to the J-coupling between protons in H_2O and $NaBH_4$ via hydrogen bonds.[26,27] This hydrogen-bond mediated J-coupling also shifts the H_2O resonance from 4.6 to 4.0 ppm with a doublet splitting of 34 Hz. The relatively large J-coupling interactions between H_2O and $NaBH_4$ suggests a very short distance between protons from H_2O and those from $NaBH_4$, ~ 1.8 Å.[26,27] The ^{1}H NMR of the $NaBH_4$ + H_2O/D_2O also indicates very little or no reactions occurring between $NaBH_4$ and H_2O in the absence of the catalyst, despite the short spatial distance between them. No freely tumbling H_2O peak is observed at 4.6 ppm, due to the fact that H_2O is a very minor component in the mixture of H_2O/D_2O and the source of H_2O is only through absorption of H_2O in the air into the D_2O solvent.

The ^{1}H solid-state NMR spectrum of Co-HNP + H_2O/D_2O + $NaBH_4$ shows two peaks, one at 4.6 ppm from freely tumbling H_2O and the other at 5.7 ppm from OH^-. This spectrum unveils the results of the Co-HNP catalyzed reaction between H_2O and $NaBH_4$.

$$4H_2O + NaBH_4 \rightarrow 4H_2 + NaB(OH)_4$$

In this reaction, H_2O is the access reagent, which consumes all $NaBH_4$ and eliminates all Co−H. Therefore, no $NaBH_4$ or Co−H ^{1}H resonance is seen in the ^{1}H spectrum of Co-HNP + H_2O/D_2O + $NaBH_4$.

In summary, the systematic series of ^{1}H NMR spectra in Figure 3a lead to the following inferences:

(1) Co−H is formed;
(2) H_2O can react with Co−H in the absence of $NaBH_4$, leading to the formation of H_2 and Co−OH;
(3) H_2O does not directly react with $NaBH_4$ without Co-HNP.

Therefore, the H^- ions have to be first transferred from $NaBH_4$ to Co-HNP to form Co−H and then combine with H^+ from H_2O to eventually form H_2. These two steps are sequential.

The evidence for the H^- transfer step can be further found from analyzing the ^{1}H spectra of $NaBH_4$ alone and Co-HNP + $NaBH_4$ in more details. As shown in Figure 3b, the ^{1}H spectrum of $NaBH_4$ alone is composed of three components: one resonance at −0.2 ppm from $NaBH_4$, one at 4.5 ppm from H_2O/OH hydrogen-bonded to $NaBH_4$, and the other at ca. −5 ppm from $NaBH_4$ hydrogen-bonded to H_2O. Compared with the ^{1}H resonances of H_2O and $NaBH_4$ without hydrogen bonding, the resonances for hydrogen-bonded H_2O and $NaBH_4$ shift to higher field (smaller ppm values) and are significantly broader. The upper-field shift is due to the shielding effect as a result of increased electron density between the hydrogen-bonded protons.[26,27] The broader peak width is a result of exchange between non-hydrogen bonded protons with hydrogen-bonded protons on the NMR time scale.[26,27] For instance, adjacent non-hydrogen-bonded $NaBH_4$ protons at −0.2 ppm chemically exchanges with hydrogen-bonded $NaBH_4$ protons at −7 ppm can lead to a broad resonance with a population-weighted-average shift at −5 ppm. The same can be deduced for exchange between non-hydrogen bonded with hydrogen-bonded H_2O protons. Based on the area integral of the deconvoluted ^{1}H spectrum of $NaBH_4$, $NaBH_4$ accounts for 88 atom %, $NaBH_4$ hydrogen-bonded to H_2O accounts for 9 atom %, and H_2O hydrogen-bonded to $NaBH_4$, accounts for 3 atom % of total protons in the $NaBH_4$ sample. Again, the ^{1}H NMR spectrum of $NaBH_4$ with minor H_2O absorbed from air suggests that H_2O and $NaBH_4$ coexist in a close proximity (<1.8 Å), very little reaction occurs without catalysts. The ^{1}H NMR spectrum of Co-HNP + $NaBH_4$ also shows three components (Figure 3c): the −0.2-ppm resonance is from $NaBH_4$, the one at 4.5 ppm is from OH hydrogen-bonded to $NaBH_4$, and the other at ca. −3.4 ppm is from hydrides hydrogen-bonded to OH. There are two distinct differences between the ^{1}H spectra of $NaBH_4$ alone and Co-HNP + $NaBH_4$, i.e., the shifts and the amount of hydrides hydrogen-bonded to H_2O/OH. The lower-field shift at −3.4 ppm in Co-HNP + $NaBH_4$ suggests a different type of hydride, instead of

DOI: 10.1021/acs.jpcc.7b03094
J. Phys. Chem. C 2017, 121, 12610−12616

$NaBH_4$, it is likely to be Co−H. Since the coexistence of $NaBH_4$ and H_2O in the presence of Co-HNP is very unlikely, the 4.5-ppm resonance should be from OH^-, which is shifted from 5.7 ppm due to hydrogen bonding to hydrides. Closer examination of the 4.5-ppm resonance in both samples reveals that the line width is twice broader for the Co-HNP + $NaBH_4$ sample than for the $NaBH_4$ alone, which supports the hydrogen bond hypothesis. Compared to H_2O, OH^- is a weaker proton donor to Co−H, thus the hydrogen bonding is expected to be weaker, thus the effect of shifting the Co−H resonance to higher field (more negative ppm values) is not as strong as observed in the $NaBH_4$ sample with minor absorbed H_2O. Therefore, the Co−H resonance is shifted from the original position at −2 ppm to −3.4 ppm due to its hydrogen-bond to OH. The significant amount of protons in Co−H, 32 atom % indicates the hydride transfer from $NaBH_4$ to Co.

The ^{11}B NMR spectra in Figure 4 support the conclusions that have been drawn from ^1H NMR in Figure 3. The ^{11}B NMR

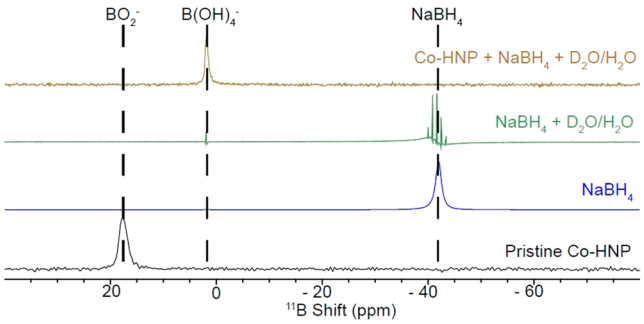

Figure 4. Solid-state ^{11}B NMR spectra of samples with different combinations of Co-HNP, $NaBH_4$, and H_2O/D_2O.

spectrum of pristine Co-HNP shows a single resonance at 17 ppm, assigned to residual BO_2^- from the synthesis process. The broad peak of $NaBH_4$ appears at −42 ppm. The addition of D_2O/H_2O to $NaBH_4$ leads to a better resolution showing multiplets due to $^1H-^{11}B$ J-coupling and a very small resonance at 2 ppm from $B(OH)_4^-$ as a result of minor reactions between H_2O and $NaBH_4$. The solid-state ^{11}B NMR spectrum of Co-HNP + H_2O/D_2O + $NaBH_4$ only shows the resonance of $B(OH)_4^-$, a product from the catalyzed reaction between H_2O and $NaBH_4$.

Based on these solid-state NMR data, a catalytic mechanism by which Co-HNP promotes the hydrolysis of $NaBH_4$ is proposed: BH_4^- interacts with Co-HNP and transfers H^- to Co to form Co−H; water is bound to Co-HNP and activated, which provides proton to react with Co−H to form H_2; the formed OH groups are bound to Co-HNP, which would react with boron species, leading to the formation of surface bound borate; the surface bound borate would slowly dissolve into solution, and the catalytic active sites are regenerated. This study helps to distinguish various mechanisms proposed in the literature regarding catalytic hydrolysis of $NaBH_4$, and the resulting experimental evidence supports the Michaelis−Menten mechanism proposed by Guella et al. for the hydrolysis of $NaBH_4$ on palladium.[20]

CONCLUSION

In summary, we have achieved a simple and low-cost Co-HNP catalyst with high activity and good reusability for the catalytic hydrolysis of sodium borohydride. The synergistic effect between Co and doping elements together with the unique hollow nanostructure leads to the excellent catalytic activity of the Co-HNP, which is superior to those of most previously reported non-noble metal catalysts. Solid state NMR was used to probe the catalytic mechanism of hydrolysis of SBH, which suggests the key role of Co-HNP in the activation of both BH_4^- and water, leading to accelerated reactions. Therefore, Co-HNP can serve as a highly active, robust and low-cost catalyst to promote the usage of SBH as practical hydrogen-storage materials for clean energy applications. In addition, the correlation of Co-NHP's activity for electrocatalytic hydrogen generation from water[18] and Co-NHP's activity for hydrogen generation from SBH hydrolysis is well demonstrated. Therefore, novel high-performance catalysts for hydrogen generation reactions may be developed by exploring known electrocatalysts for hydrogen generation reactions, and vice versa.

ASSOCIATED CONTENT

Supporting Information

The Supporting Information is available free of charge on the ACS Publications website at DOI: 10.1021/acs.jpcc.7b03094.

Characterization data (SEM, TEM, XPS, Raman, XRD) of Co-HNP, Co-SNP, and Amorphous-Co samples; catalytic activity data of these Co-based catalysts at different conditions (PDF)

AUTHOR INFORMATION

Corresponding Authors

*E-mail: mma@ustc.edu.cn.
*E-mail: hu@chem.fsu.edu.

ORCID

Mingming Ma: 0000-0002-7967-8927

Notes

The authors declare no competing financial interest.

ACKNOWLEDGMENTS

This work was supported by the National Natural Science Foundation of China (21474094, 81401531) and the Natural Science Foundation of Anhui Province (1508085QH154). Acknowledgement is made to the Donors of the American Chemical Society Petroleum Research Fund, for partial support of this research.

REFERENCES

(1) Schlapbach, L.; Züttel, A. Hydrogen-storage Materials for Mobile Applications. *Nature* **2001**, *414*, 353−358.
(2) Zhu, Q.; Xu, Q. Liquid Organic and Inorganic Chemical Hydrides for High-capacity Hydrogen Storage. *Energy Environ. Sci.* **2015**, *8*, 478−512.
(3) Umegaki, T.; Yan, J.; Zhang, X.; Shioyama, H.; Kuriyama, N.; Xu, Q. Boron- and Nitrogen-based Chemical Hydrogen Storage Materials. *Int. J. Hydrogen Energy* **2009**, *34*, 2303−2311.
(4) Demirci, U.; Miele, P. Sodium Borohydride versus Ammonia Borane, in Hydrogen Storage and Direct Fuel Cell Applications. *Energy Environ. Sci.* **2009**, *2*, 627−637.
(5) Mori, K.; Miyawaki, K.; Yamashita, H. Ru and Ru-Ni Nanoparticles on TiO_2 Support as Extremely Active Catalysts for Hydrogen Production from Ammonia-Borane. *ACS Catal.* **2016**, *6*, 3128−3135.
(6) Chen, W.; Duan, X.; Qian, G.; Chen, D.; Zhou, X. Carbon Nanotubes as Support in the Platinum-Catalyzed Hydrolytic

Dehydrogenation of Ammonia Borane. *ChemSusChem* **2015**, *8*, 2927−2931.
(7) Tonbul, Y.; Akbayrak, S.; Ozkar, S. Palladium(0) Nanoparticles Supported on Ceria: Highly Active and Reusable Catalyst in Hydrogen Generation from the Hydrolysis of Ammonia Borane. *Int. J. Hydrogen Energy* **2016**, *41*, 11154−11162.
(8) Wang, H.; Zhao, Y.; Cheng, F.; Tao, Z.; Chen, J. Cobalt Nanoparticles Embedded in Porous N-doped Carbon as Long-life Catalysts for Hydrolysis of Ammonia Borane. *Catal. Sci. Technol.* **2016**, *6*, 3443−3448.
(9) Wang, Y.; Qi, K.; Wu, S.; Cao, Z.; Zhang, K.; Lu, Y.; Liu, H. Preparation, Characterization and Catalytic Sodium Borohydride Hydrolysis of Nanostructured Cobalt-Phosphorous Catalysts. *J. Power Sources* **2015**, *284*, 130−137.
(10) Wang, Y.; Li, T.; Bai, S.; Qi, K.; Cao, Z.; Zhang, K.; Wu, S.; Wang, D. Catalytic Hydrolysis of Sodium Borohydride via Nanostructured Cobalt-Boron Catalysts. *Int. J. Hydrogen Energy* **2016**, *41*, 276−284.
(11) Patel, N.; Fernandes, R.; Miotello, A. Hydrogen Generation by Hydrolysis of $NaBH_4$ with Efficient Co-P-B Catalyst: A Kinetic Study. *J. Power Sources* **2009**, *188*, 411−420.
(12) Fernandes, R.; Patel, N.; Miotello, A. Efficient Catalytic Properties of Co-Ni-P-B Catalyst Powders for Hydrogen Generation by Hydrolysis of Alkaline Solution of $NaBH_4$. *Int. J. Hydrogen Energy* **2009**, *34*, 2893−2900.
(13) Dai, H.; Liang, Y.; Wang, P. Effect of Trapped Hydrogen on the Induction Period of Cobalt-Tungsten-Boron/Nickel Foam Catalyst in Catalytic Hydrolysis Reaction of Sodium Borohydride. *Catal. Today* **2011**, *170*, 27−32.
(14) Kang, J.; Chen, T.; Zhang, D.; Guo, L. PtNiAu Trimetallic Nanoalloys Enabled by a Digestive-Assisted Process as Highly Efficient Catalyst for Hydrogen Generation. *Nano Energy* **2016**, *23*, 145−152.
(15) Liu, B.; Li, Z.; Suda, S. Nickel- and Cobalt-based Catalysts for Hydrogen Generation by Hydrolysis of Borohydride. *J. Alloys Compd.* **2006**, *415*, 288−293.
(16) Arzac, G.; Hufschmidt, D.; Jiménez De Haro, M.; Fernández, A.; Sarmiento, B.; Jiménez, M.; Jiménez, M. Deactivation, Reactivation and Memory Effect on Co-B Catalyst for Sodium Borohydride Hydrolysis Operating in High Conversion Conditions. *Int. J. Hydrogen Energy* **2012**, *37*, 14373−14381.
(17) Liu, B. H.; Li, Q. A Highly Active Co-B Catalyst for Hydrogen Generation from Sodium Borohydride Hydrolysis. *Int. J. Hydrogen Energy* **2008**, *33*, 7385−7391.
(18) Kim, D.; Cho, K.; Choi, Y.; Park, C. Fabrication of Porous Co-Ni-P Catalysts by Electrodeposition and Their Catalytic Characteristics for the Generation of Hydrogen from an Alkaline NaBH4 Solution. *Int. J. Hydrogen Energy* **2009**, *34*, 2622−2630.
(19) Liu, B.; Zhang, L.; Xiong, W.; Ma, M. Cobalt-Nanocrystal-Assembled Hollow Nanoparticles for Electrocatalytic Hydrogen Generation from Neutral-pH Water. *Angew. Chem., Int. Ed.* **2016**, *55*, 6725−6729.
(20) Guella, G.; Zanchetta, C.; Patton, B.; Miotello, A. New Insights on the Mechanism of Palladium-Catalyzed Hydrolysis of Sodium Borohydride from B-11 NMR Measurements. *J. Phys. Chem. B* **2006**, *110*, 17024−17033.
(21) Arzac, G.; Rojas, T.; Fernández, A. Boron Compounds as Stabilizers of a Complex Microstructure in a Co-B-based Catalyst for $NaBH_4$ Hydrolysis. *ChemCatChem* **2011**, *3*, 1305−1313.
(22) Walter, J. C.; Zurawski, A.; Montgomery, D.; Thornburg, M.; Revankar, S. Sodium Borohydride Hydrolysis Kinetics Comparison for Nickel, Cobalt, and Ruthenium Boride Catalysts. *J. Power Sources* **2008**, *179*, 335−339.
(23) Dai, H.; Liang, Y.; Ma, L.; Wang, P. New Insights into Catalytic Hydrolysis Kinetics of Sodium Borohydride from Michaelis-Menten Model. *J. Phys. Chem. C* **2008**, *112*, 15886−15892.
(24) Seven, F.; Sahiner, N. Superporous P(2-Hydroxyethyl Methacrylate) Cryogel-M (M:Co, Ni, Cu) Composites as Highly Effective Catalysts in H_2 Generation from Hydrolysis of $NaBH_4$ and NH_3BH_3. *Int. J. Hydrogen Energy* **2014**, *39*, 15455−15463.
(25) Retnamma, R.; Novais, A.; Rangel, C. Kinetics of Hydrolysis of Sodium Borohydride for Hydrogen Production in Fuel Cell Applications: A Review. *Int. J. Hydrogen Energy* **2011**, *36*, 9772−9790.
(26) Epstein, L.; Shubina, E. New Types of Hydrogen Bonding in Organometallic Chemistry. *Coord. Chem. Rev.* **2002**, *231*, 165−181.
(27) Belkova, N.; Epstein, L.; Filippov, O.; Shubina, E. Hydrogen and Dihydrogen Bonds in the Reactions of Metal Hydrides. *Chem. Rev.* **2016**, *116*, 8545−8587.

DOI: 10.1021/acs.jpcc.7b03094
J. Phys. Chem. C 2017, 121, 12610−12616